Electric Power Systems Research 212 (2022) 108527

Contents lists available at ScienceDirect

Electric Power Systems Research

journal homepage: www.elsevier.com/locate/epsr

# Step detection in power system waveforms for improved RoCoF and frequency estimation☆

Alexandra Karpilow [a,*], Asja Derviškadić [b], Guglielmo Frigo [c], Mario Paolone [a]

[a] Distributed Electrical Systems Laboratory, École Polytechnique Fédérale de Lausanne (EPFL), Lausanne, Switzerland
[b] Swissgrid Ltd., Aarau, Switzerland
[c] METAS, Bern, Switzerland

ARTICLE INFO

*Keywords:*
Amplitude and phase steps
Compressed sensing
Event detection
Frequency
Power system dynamics

ABSTRACT

The evaluation of the signal frequency and Rate of Change of Frequency (RoCoF) from voltage or current waveforms is used for critical grid control, monitoring and protection applications. However, when step changes in the amplitude or phase of the signal occur, conventional frequency and RoCoF estimation methods, typically based on phasor models, are highly unreliable and can yield large frequency errors. To address this issue, this paper proposes a technique that uses dictionaries based on common signal dynamic models to identify and track amplitude and/or phase steps in AC signals. Additional signal dynamics including amplitude modulations, frequency ramps and harmonic tones are also characterized. Distinct from a previous iteration of this method developed by the authors, the proposed Step Change Detection (SCD) technique separates the envelope and angle of the signal's analytic form for independent analysis of these components. For numerical validation the method is applied to synthetically generated signals with challenging combinations of signal dynamics. The technique is shown to greatly improve frequency and RoCoF approximations as compared to state-of-the-art phasor estimation methods.

## 1. Introduction

In modern power grids, the presence of step changes in the amplitude and/or phase of AC voltage or current waveforms is challenging for conventional measurement algorithms and protection schemes relying on phasors. Commonly caused by network reconfigurations, circuit breaker operations or faults, steps can be misinterpreted as large deviations in the frequency or Rate of Change of Frequency (RoCoF). In distribution systems, this can lead to false triggering of Loss-of-Mains (LOM) protection and errors in synthetic inertia calculations [1]. For transmission systems, as discussed in [2], frequency and RoCoF are typically used to determine load shedding quantities to reduce the chance of cascading blackouts, generation loss or grid separation. Errors in the estimation of these measurements due to the presence of phase/amplitude steps can result in inappropriate Under-Frequency Load Shedding (UFLS) actions [2].

To exemplify the risks posed by misinterpreting measurements with phase or amplitude steps, when a fault on the transmission circuit in the California grid in 2017 resulted in a series of phase steps, the inverters connecting a number of solar power plants were tripped due to erroneous instantaneous frequency estimates and 700 MW of generation was lost [3]. Separately, a study of LOM triggered events in the Bornholm Island grid in the Baltic Sea, a grid characterized by high penetration of wind generation, found a number of false RoCoF triggers were due to phase shifts in the waveforms rather than underlying frequency dynamics [4].

The IEEE Std. C37.118 [5] specifies performance requirements for Phasor Measurement Units (PMUs) during dynamic conditions and distinguishes between P (Protection) and M (Measurement) class algorithms. Briefly, P class PMUs prioritize response time at the expense of accuracy in order to adapt to rapidly varying conditions. M class PMUs offer better accuracy and robustness to inter-harmonics but are slow to respond to dynamic changes. Fundamentally, these trade-offs acknowledge that the phasor model poorly represents waveforms with transients, particularly fast variations like step changes. As investigated in [1,6–8], the narrowband phasor model is inherently unqualified to capture broadband signal dynamics since the spectrum of these time-varying waveforms is no longer concentrated at a single frequency component. Abrupt transitions of phase and amplitude can

☆ The authors gratefully acknowledge the financial support of the European Commission - Horizon 2020 program to the project Optimal System-Mix Of flexibility Solutions for European electricity (OSMOSE) (773406).

* Corresponding author.
*E-mail address:* alexandra.karpilow@epfl.ch (A. Karpilow).

https://doi.org/10.1016/j.epsr.2022.108527
Received 8 October 2021; Received in revised form 15 April 2022; Accepted 2 July 2022
Available online 21 July 2022

result in misleading synchrophasor estimations and inappropriate control actions [7]. Indeed, during the grid event in California, the synchrophasors reported by a PMU during this event failed to capture the true nature of the waveforms and, instead, reported large frequencies deviations [3].

Recent literature has proposed various signal processing techniques to better analyze waveform measurements involving transient behavior. Significant research has been conducted on dynamic phasor methods based on Taylor series expansions or Taylor–Fourier series which can capture higher order phasor derivatives for improved dynamic representation [9,10]. Alternatively, many proposed methods focus on detecting step transitions in order to flag the phasor estimations as invalid. In [11], a step detection algorithm is based on the instantaneous amplitude and frequency of the analytic signal, using threshold and median operators. However, the method only identifies the step location and provides a rough approximation of the underlying frequency but does not characterize the full signal dynamic. In [12], the authors employ a Kalman Filter and compare the predicted waveform to the true input in order to detect sudden transients. The performance of the method on slower dynamics (e.g., frequency ramps, amplitude modulations) and identification of the type of discontinuity (e.g., phase or amplitude steps) is not discussed. In [13], wavelet analysis is used to first identify the location of discontinuities in the waveform. Next, an adaptive windowing technique is applied to fit a quadratic polynomial signal model to the pre- and post-event data. Despite promising results, the adequacy of this fitting method in the presence of multiple steps or additional harmonics is still to be investigated. In [14], a nonlinear least-squares estimator and a model of the step are used in order to accurately capture the signal dynamic, a method that is expanded on in [15]. However, these techniques are not practical for real-time applications and may be invalid in the presence of additional signal dynamics like amplitude modulations or frequency ramps.

Adding to this research, this paper proposes a method for the detection and identification of amplitude and phase steps in voltage or current waveforms. Building off of the study in [16], which presents the Functional Basis Analysis (FBA) algorithm for the characterization of signal dynamics, the proposed Step Change Detection (SCD) technique employs a dictionary of parameterized signal models in order to identify the location and magnitude of step dynamics as well as characterize other modulations in the signal (e.g., frequency ramps, amplitude modulations, interfering tones). The SCD technique has reduced computational cost and improved flexibility as compared to the original FBA method, making it more suited for eventual implementation in Field-Programmable Gate Array (FPGA) devices for real-time applications. As compared to the other dynamic signal processing techniques discussed above which attempt to remove, minimize or ignore the impact of step changes, the proposed method aims to obtain a model that incorporates these disturbances and is therefore better representative of the true signal dynamic. The parameters of the identified steps and the improved RoCoF estimation could be potentially incorporated into automated decision making strategies for the control and protection of modern power grids.

The paper is organized as follows: Section 2 explores the theory behind analytic signals and models of common signal dynamics in power grids. In Section 3, we present the SCD algorithm for analysis of the signal envelope and frequency, as well as discuss the computational complexity of the method. Section 4 provides the numerical validation of the SCD technique by applying it to various signal dynamic combinations. The results are compared to both static and dynamic phasor estimation methods. Finally, Section 5 concludes the paper with a discussion of the potential applications of the method and the additional research required to make it practical.

## 2. Theory and mathematical background

The objective of this paper is to identify and characterize step dynamics in power system signals for improved frequency and RoCoF analysis. The conventional phasor model assumes a fixed amplitude, phase and frequency for the duration of the observation window. For steady-state or slowly transitioning waveforms (i.e., quasi-steady state where the amplitude and frequency change gradually), a phasor is sufficient to approximate the signal parameters. However, this model is inherently incapable of capturing fast signal dynamics, often resulting in extremely inaccurate approximations of the underlying signal parameters.

As discussed, phasors are narrowband signal models where the energy content is concentrated around a single frequency component, as seen in Fig. 1. In contrast, the frequency spectrum of waveforms containing amplitude (AS) or phase steps (PS) is broadband and continuous. Consequently, phasor extraction algorithms that involve direct analysis of the frequency spectrum and assume a narrowband spectrum (e.g., interpolated discrete Fourier Transform techniques) are significantly biased by these disturbances.

To address these problems, we propose to adapt the signal model to incorporate step discontinuities for improved signal analysis in the presence of fast dynamics. Power system signals can be generically modeled as:

$$x(t) = A_0(1 + g_A(t))cos(2\pi f_0 t + g_\phi(t)) \tag{1}$$

where $A_0$, $f_0$ and $\phi_0$ represent the fundamental amplitude, frequency and phase, respectively, and $g_A$ and $g_\phi$ incorporate variations in the amplitude and phase.

Similar to how phasors are often represented as complex exponentials, (1) can be transformed into its analytic signal counterpart using the Hilbert Transform (HT). As is known, the HT is a linear operator that, for a generic time-varying signal $x(t)$, is defined as [17]:

$$\mathcal{H}[x(t)] = \frac{1}{\pi}\int_{-\infty}^{+\infty}\frac{x(\tau)}{t-\tau}d\tau = \frac{1}{\pi t} * x(t) \tag{2}$$

where $*$ indicates convolution. Combining the HT $\mathcal{H}[x(t)]$ with the original function yields the analytic signal $\hat{x}(t)$ which, due to the symmetry of the spectrum, contains only positive frequency components [17]:

$$\hat{x}(t) = x(t) + j\mathcal{H}(x(t)). \tag{3}$$

Applying Euler's formula, the analytic form (3) allows for the representation of a real time-domain signal (1) as a complex exponential function:

$$\hat{x}(t) = A_0(1 + g_A(t))e^{j(2\pi f_0 t + g_\phi(t))} \tag{4}$$

which contains information on the signal envelope $x_A(t)$ and phase $x_\phi(t)$ where:

$$x_A(t) = |\hat{x}(t)| \tag{5}$$

$$x_\phi(t) = \angle\hat{x}(t). \tag{6}$$

The instantaneous frequency of the signal is defined as:

$$x_f(t) = \frac{1}{2\pi}\frac{dx_\phi(t)}{dt}. \tag{7}$$

The separation of the envelope and phase/frequency of the signal allows for independent analysis of these components, as discussed in the next section.

Along with AS and PS, power grids are likely to experience amplitude modulations (AM) and frequency ramps (FR). For reference, the analytic model for each of these dynamics can be formulated as [18]:

$$\hat{x}_{AS}(t) = A_0(1 + k_s h(t - t_s))e^{j(2\pi f_0 t)} \tag{8}$$

$$\hat{x}_{PS}(t) = A_0 e^{j(2\pi f_0 t + k_p h(t - t_p))} \tag{9}$$

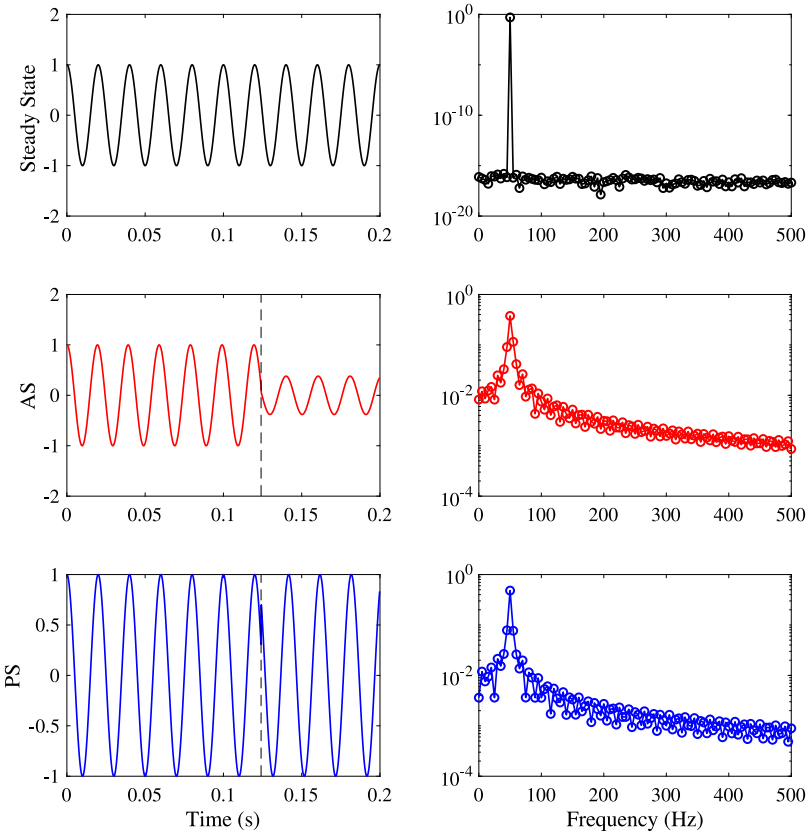


**Fig. 1.** Time domain waveform and frequency spectrum of 200 ms signals at 50 Hz in steady state (black), with an amplitude step $k_s = -62\%$ (red) or a phase step $k_p = -3\pi/18$ (blue).

$$\hat{x}_{AM}(t) = A_0(1 + k_m cos(2 * \pi f_m t + \varphi_m))e^{j(2\pi f_0 t)} \tag{10}$$

$$\hat{x}_{FR}(t) = A_0 e^{j(2\pi f_0 t + R\pi t^2)} \tag{11}$$

where $h(t)$ is the Heaviside function, $k_s$ and $k_p$ are the step depths, $t_s$ and $t_p$ are the step locations within the window, $k_m$, $f_m$ and $\varphi_m$ represent the AM depth, frequency and phase, respectively, and $R$ is the ramp rate in Hz/s. Eqs. (8)–(11) are derived using the property that the HT of the product of two signals with non-overlapping spectra is equal to the product of the low-frequency term and the HT of the high-frequency term (see [18] for further details).

## 3. Signal analysis

For the identification and characterization of signal dynamics using the models previously discussed, we turn to the field of *Compressed Sensing* where dictionaries of functions are used to characterize input signals. Fundamentally, dictionary analysis involves projection of the input vector (i.e., a sampled, windowed signal) onto a functional basis of vectors defined by parameterized signal models. The kernel that best matches the input signal is identified and its corresponding parameters and model are used to reconstruct the input signal.

The proposed algorithm exploits this concept of parameterized dictionaries to characterize the input waveform. As detailed in Algorithms 1 and 2, the envelope and instantaneous frequency of the input analytic signal are analyzed separately. These signal components are projected onto relevant dictionaries (e.g., the signal envelope is projected onto AM and AS dictionaries) and the closest matching dictionary kernel is identified with its corresponding model parameters. Note that the analytic form of the input waveform must first be approximated by a proper Hilbert-type filter, the definition of which is beyond the scope of this paper. For this reason synthetic analytic signals are used for testing in Section 4.

### 3.1. Envelope analysis

The signal envelope can be approximated by modulations or steps in the amplitude and is therefore modeled as

$$\text{AM: } x_A(t) = A_0(1 + k_m cos(2\pi f_m t + \varphi_m)) \tag{12}$$

$$\text{AS: } x_A(t) = A_0(1 + k_s h(t_s)). \tag{13}$$

As shown in Algorithm 1, two dictionaries (AM and AS) are applied in parallel to analyze the signal envelope.

The AM dictionary is defined for all combinations of the frequency $f_m$ and phase $\varphi_m$ parameters:

$$d_{i,AM}(f_m, \varphi_m) = a_i DFT[cos(2\pi f_m t + \varphi_m)] \tag{14}$$

where $a_i$ is a coefficient that normalizes the kernel and DFT indicates the Discrete Fourier Transform. DFT coefficients for bins $k = 0...K-1$ are defined as:

$$X(k) = DFT[x(t_l)] = \sum_{l=0}^{L-1} x(t_l) W_L^{kl} \tag{15}$$

where $W_L^k = e^{-j2\pi k/L}$ is the $k$th root of unity modulo $L$. Each kernel is then fully determined by the parameter set $\gamma(f_m, \varphi_m)$ and signal model of the envelope for a sampled window $t_l$ where $l = 0...L-1$.

Similarly, the AS dictionary is composed of kernels $d_i$ at different step locations $t_s$:

$$d_{i,AS}(t_s) = a_i DFT[h(t_l - t_s)]. \tag{16}$$

The parameter sets $\gamma_{AS} = [t_s]$ and $\gamma_{AM} = [f_m, \varphi_m]$ are selected to best capture common signal dynamics in power grids (e.g., $f_m \in [0, 5]$ Hz). The parameter set resolutions are also user-defined and depend on performance requirements and the computational cost of the algorithm.

Note that the DFT of the envelope is used rather than the time-domain waveform since this allows for the compression of the signal into a reduced set of Fourier coefficients. Examination of these coefficients allows for the extraction of the remaining model parameters, such as the scaling factor of the dynamic (i.e., $A_0 k_s$ or $A_0 k_m$) and the DC shift (i.e., $A_0$). For this reason, kernels in the AS and AM dictionaries are defined for frequency ranges that exclude the DC component (i.e., $k = 1...K-1$).

The analysis of the signal envelope is detailed in Algorithm 1 where the frequency spectrum of the signal envelope is first computed and curtailed to the appropriate frequency range (e.g., 0 to 100 Hz). This range is user-defined and selected to best capture the signal dynamics of interest. In lines 3–5, the DC component is separated ($X_{A,DC}$) while the remaining frequency bins are normalized by either the length of the window $L$ or the norm of the vector (i.e., $a = \|X_{full}(k = 1...K-1)\|_2^{-1}$) to yield $X_A$ and $\bar{X}_A$, respectively. The latter is then projected onto all kernels in the envelope dictionaries and the kernel that minimizes the objective function $\|\mathbf{d}_{i,j}^H \bar{X}_A \mathbf{d}_{i,j} - \hat{X}\|_2$ is identified. The corresponding parameter sets for AM and AS dynamics are identified in lines 6 and 14, respectively.

In lines 7–8 and 15–16, the parameter sets $\gamma_{AM}^*$ and $\gamma_{AS}^*$ and the frequency vector $X_A$ are used to calculate the combined scaling factors, $c_{AS} = k_s A_0$ and $c_{AM} = k_m A_0$. $A_0$ is then computed in lines 9–10 and 17–18 by removing the spectral leakage due to the presumed dynamic ($X_2(k = 0)$) from the DC component $X_{A,DC}$. With $A_0$, the combined scaling factors, $c_{AM}$ and $c_{AS}$, can be used to identify $k_m$ and $k_s$ in lines 11 and 19, respectively.

The envelopes are then reconstructed in lines 12 and 20 and compared to the original envelope using the Time-Domain Error (TDE) metric:

$$TDE(x^*, x) = \frac{\|x^*(t_l) - x(t_l)\|_2}{\sum_{l=0}^{L-1} x(t_l)^2}, \tag{17}$$

The envelope with the smaller TDE is reported as the most likely amplitude dynamic (i.e., amplitude modulation or amplitude step). Thresholds on the minimum magnitude (i.e., $k_m$, $k_s$) and location $t_s$ of the respective signal dynamics can be set by the user to avoid reporting insignificant variations. In steady-state conditions, for instance, the "detected" AS dynamic may have a very small magnitude or a step located at $t_s = 0$ or $t_s = T_w$.

**Algorithm 1** Envelope Analysis

1: **Input:** Signal envelope $x_A(t_l)$,
Envelope dictionaries $\mathbf{D}_{AS}$, $\mathbf{D}_{AM}$
2: $X_{A,full} = DFT[x_A(t_l)]$
3: $X_A = X_{A,full}(k = 1...K-1)/L$
4: $\bar{X}_A = aX_{full}(k = 1...K-1)$
5: $X_{A,DC} = X_{full}(k = 0)/L$

AM DETECTION:
**Project onto kernels $\mathbf{d}_{i,j}$ in dictionary $\mathbf{D}_{AM}$**
6: $[i^*, j^*] = \text{argmin}_{i,j}[\|\mathbf{d}_{i,j}^H \bar{X}_A \mathbf{d}_{i,j} - \hat{X}\|_2]$
$\rightarrow \gamma_{AM}^* = [f_m(i^*), \varphi_m(j^*)]$,
**Calculate scaling factor ($k_m A_0$)**
7: $X_{AM,1} = DFT[sin(2\pi f_m^* t_l + \varphi_m^*)]/L$
8: $c_{AM} = |X_{AM,1}^H X_A|$
**Calculate DC shift ($A_0$)**
9: $X_{AM,2} = DFT[c_{AM} sin(2\pi f_m^* t_l + \varphi_m^*)]/L$
10: $A_0^* = X_{A,DC} - X_{AM,2}(k = 0)$
11: $k_m^* = c_{AM}/A_0^*$
12: $x_{AM}^* = A_0^*(1 + k_m^* sin(2\pi f_m^* t_l + \varphi_m^*))$
13: Compute $TDE(x_{AM}^*, x_A)$

AS DETECTION:
**Project onto kernels $\mathbf{d}_i$ in dictionary $\mathbf{D}_{AS}$**
14: $[i^*] = \text{argmin}_i[\|\mathbf{d}_i^H \bar{X}_A \mathbf{d}_i - \hat{X}\|_2]$
$\rightarrow \gamma_{AS}^* = [t_s(i^*)]$,
**Calculate scaling factor ($k_s A_0$)**
15: $X_{AS,1} = DFT[h(t_l - t_s^*)]/L$
16: $c_{AS} = |X_{AS,1}^H X_A|$
**Calculate DC shift ($A_0$)**
17: $X_{AS,2} = DFT[c_{AS} h(t_l - t_s^*)]/L$
18: $A_0^* = X_{A,DC} - X_{AS,2}(k = 0)$
19: $k_s^* = c_{AS}/A_0^*$
20: $x_{AS}^* = A_0^*(1 + k_s^* h(t_l - t_s^*))$
21: Compute $TDE(x_{AS}^*, x_A)$
22: TDE comparison.

### 3.2. Frequency analysis

Any underlying frequency dynamics are analyzed in Algorithm 2 using the analytic signal and the instantaneous frequency defined in (7). Phase steps correspond to a large spike in the instantaneous frequency of the signal. The location of the peak is first identified in lines 4 and 5 by applying a detection threshold (e.g., $f_{lb} = 30$ Hz, $f_{ub} = 70$ Hz).

For PS identification, a dictionary is pre-defined for parameter sets $\gamma_{PS} = [f_0, k_p, t_p]$:

$$\mathbf{d}_{i,PS}(f_0, k_p, t_p) = a_i DFT[exp(j(2\pi f_0 t_l + k_p h(t_l - t_p)))] \tag{18}$$

While this dictionary is quite large due to the high resolution of the $t_p$ parameter set, the step location identified in line 5 allows for a slice of the dictionary to be used, $\gamma_{PS} = [f_0, k_p]_{t_p^*}$ The frequency spectrum of the analytic signal $\hat{X}$ is then projected onto this subset of the PS dictionary. Once the phase step is fully characterized, it is removed in line 7, leaving the instantaneous frequency $x_f(t_l)$ unaffected. The DFT of the instantaneous frequency is then computed, normalized and projected onto a FR dictionary with kernels defined for different ramp rates:

$$\mathbf{d}_{i,FR}(R) = a_i DFT[Rt_l] \tag{19}$$

The best matching ramp rate (found in line 11) together with the DC shift (i.e., the magnitude of the DC component in line 10) are used to find the fundamental frequency at the beginning of the window, as shown in line 12. The reconstructed analytic signal and its frequency spectrum are then computed in line 15, incorporating the estimated amplitude envelope from Algorithm 1, any identified PS and the underlying FR. Finally, the initial phase of this signal is the angle of the coefficient found by projecting the spectrum of this reconstructed signal onto the spectrum of the original analytic signal (line 14). In line 16, the TDE is computed to indicate how well the resulting signal model matches the input waveform.

### 3.3. DC offset and harmonics

Additional signal components that might appear in power system waveforms include DC offsets and harmonics. The former proves problematic when converting the signal to its analytic form. The DC offset shifts only the real part of the signal since the HT of a constant is 0. Consequently, the offset introduces artificial oscillations into the extracted envelope and instantaneous frequency. To avoid this, the DC offset should be removed in the pre-processing stage by either a notch filter or other detrending techniques.

The impact of harmonics on the SCD method is also examined. Since the FR dictionary based on the instantaneous frequency is highly sensitive to these additional disturbances, an iterative method to identify and remove these dynamics is as follows:

(1) Algorithms 1 and 2 provide a first approximation of the underlying analytic signal $\hat{x}_{est}(t_l)$
(2) The remaining interfering tones are isolated $\hat{x}_r(t_l) = \hat{x}(t_l) - \hat{x}_{est}(t_l)$

**Algorithm 2** Frequency Analysis

1: **Input:** analytic signal $\hat{x}_l(t)$, signal frequency $x_f(t_l)$, Dictionaries $\mathbf{D}_{FR}$ and $\mathbf{D}_{PS}$
2: $\hat{X}_{full} = DFT[\hat{x}(t_l)]$
3: $\hat{X} = \hat{X}_{full}(k = 0...K-1)$

PS DETECTION:
**Identify step location**
4: $j^* = loc[x_f < f_{lb}$ **or** $x_f > f_{ub}]$
5: $t_p^* = t_{l=j^*}$
**Project onto kernels $\mathbf{d}_i(f_0, k_p)_{t_p^*}$ in slice $t_p^*$ of dictionary $\mathbf{D}_{PS}$**
6: $[i^*] = \text{argmin}_i[||d_i^H \hat{X} d_i - \hat{X}||_2]$
$\rightarrow \gamma_{PS}^* = [f_0(i^*), k_p(i^*)]$,
**Remove PS from instantaneous frequency**
7: $x_f(j) = x_f(j-1)$

FR DETECTION
8: $X_{full} = DFT[x_f(t_l)]/(L-1)$
9: $X_f = X_{full}(k = 1...K-1)$
10: $X_{f,DC} = X_{full}(k = 0)$
**Project onto kernels $\mathbf{d}_i$ in dictionary $\mathbf{D}_{FR}$**
11: $[i^*] = \text{argmin}_i[||\mathbf{d}_i - X_f||_2]$
$\rightarrow \gamma_{FR}^* = [R(i^*)]$,
**Calculate DC shift**
12: $f_0^* = X_{f,DC} - R^* t_{L/2}$
13: $X_{est} = DFT[x_A^*(t_l) e^{j(2\pi f_0^* t_l + R^* \pi t_l^2 + k_p^* h(t_l - t_p^*))}]/L$
**Calculate phase shift**
14: $\varphi_0^* = \angle(X_{est}^H \hat{X})$
**Reconstruct full signal**
15: $x_{est} = x_A^*(t_l) cos(2\pi f_0^* t_l + R^* \pi t_l^2 + k_p^* h(t_l - t_p^*) + \varphi_0^*)$
16: Compute $TDE(x_{est}, \mathcal{R}(\hat{x}(t_l)))$

(3) The largest interfering tone is identified via 2-point interpolated DFT (IpDFT) analysis: $\hat{x}_h(t_l) = A_h e^{j(2\pi f_h t_l + \varphi_h)}$
(4) The identified tone is removed from the original signal: $\bar{x}(t) = \hat{x}(t_l) - \hat{x}_h(t_l)$
(5) Lines 8–15 from Algorithm 2 are repeated for an improved estimation of the instantaneous frequency.
(6) These steps (2-5) are repeated to improve estimation of the interfering tone or to identify additional tones.

As an example, we analyze the signal shown in Fig. 2. The waveform has an initial fundamental frequency of 47.87 Hz with 5th and 7th harmonics at relative magnitudes of 6% and 5%, respectively.[1] Furthermore, a frequency ramp of 3.82 Hz/s is present and an amplitude and phase step occur at 42 ms with magnitudes of $k_s = -0.1842$ and $k_p = -0.8642$ rad, respectively. As shown in Table 1, the initial guess correctly identifies the AS and PS dynamics, but yields a large ROCOF error of 1.02 Hz/s. When the two harmonic tones are identified and removed, the resulting frequency error is 10.4 mHz and RFE is 0.03 Hz/s.

### 3.4. Computational complexity

The complexity of the algorithm, as presented in Table 2, depends on the following variables: the number of kernels $N$ in each dictionary, the number of samples in the signal $L$, and the number of frequency bins analyzed $K$. Calculating the frequency spectrum depends on the method used (e.g., FFT, DFT) and therefore the computational complexity of this step is represented as $\zeta$. The most computationally burdensome step involves projection of the input spectrum onto AM, AS, PS and FR dictionaries. The analysis of most of these dynamics is independent and can therefore be performed in parallel. Examples of dictionary sizes and the computation time reported in MATLAB are also included in Table 2.

[1] The total harmonic distortion (THD) of 7.8% is within the limit specified by the 50 160 Standard [19].

**Table 1**
Example of parameter errors during the detection of harmonic tones.

| Parameter error | Estimation | | |
|---|---|---|---|
| | Initial | 2nd | 3rd |
| $f_0$ (mHz) | 6.5 | 87.3 | 10.4 |
| $R$ (Hz/s) | 1.02 | 1.08 | 0.03 |
| $k_p$ (%) | −2.3 | | |
| $k_s$ (%) | −1.9 | | |
| $t_p, t_s$ (ms) | 0.4 | | |
| $A_5$ (%) | | 2.7 | |
| $f_5$ (Hz) | | 0.23 | |
| $A_7$ (%) | | | 2.4 |
| $f_7$ (Hz) | | | 0.45 |

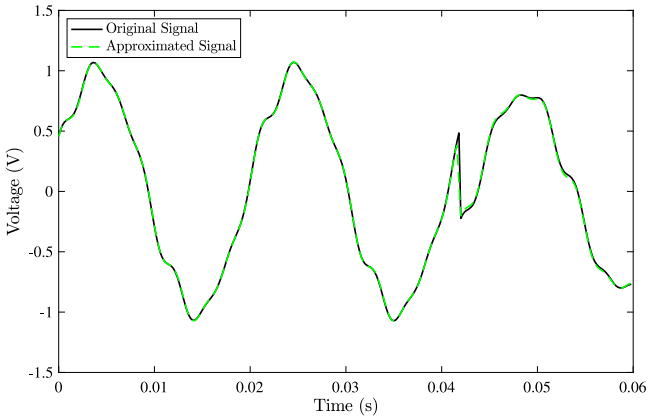


**Fig. 2.** SCD analysis of a signal with AS/PS/FR dynamics and 5th and 7th harmonics.

**Table 2**
Computational complexity of SCD steps presented in Algorithms 1 and 2.

| Dynamic | Operation | Complexity | Time (ms) | Dictionary size (N) |
|---|---|---|---|---|
| AM | Projection | $\mathcal{O}(KN)$ | 15 | 870 |
| | Scaling factor | $\mathcal{O}(L+\zeta+K)$ | 1 | |
| | DC shift | $\mathcal{O}(L+\zeta)$ | 1 | |
| AS | Projection | $\mathcal{O}(KN)$ | 3 | 150 |
| | Scaling factor | $\mathcal{O}(L+\zeta+K)$ | 2 | |
| | DC shift | $\mathcal{O}(L+\zeta)$ | 1 | |
| PS | Projection | $\mathcal{O}(KN)$ | 90 | 7272 |
| FR | Projection | $\mathcal{O}(KN)$ | 1.5 | 200 |

## 4. Numerical validation

To evaluate the performance of the algorithm, we apply it to signals with various combinations of underlying dynamics and phase/amplitude steps and compare the results to both *static* and *dynamic* phasor estimation methods. For the former, we selected a 3-point iterative Interpolated DFT (i-IpDFT) algorithm with a Hann window and negative spectrum compensation which is compliant with P and M class requirements [20]. For dynamic phasor analysis, we used the Compressed Sensing Taylor–Fourier multifrequency (CSTFM) method [10] which captures the 1st and 2nd order derivatives of the phasor. For these reference methods, the RoCoF of the signal is computed by comparing frequency estimations for consecutive windows. The proposed SCD method uses AS, AM, FR and PS dictionaries defined by the parameter sets in Table 3.

The test waveforms are generated using the analytic models described in Section 2 in order to have better control and knowledge of

**Table 3**
Parameter sets for SCD dictionaries.

| Dictionary | Parameter | Resolution | Range |
|---|---|---|---|
| PS | $f_0$ (Hz) | 0.07 | [47.5,52.5] |
| | $k_p$ (rad) | 0.014 | $\pm[\pi/18, 5\pi/18]$ |
| | $t_p$ (ms) | 0.4 | $[0, T_w]$ |
| FR | R (Hz/s) | 0.05 | [−5,5] |
| AS | $t_s$ (ms) | 0.4 | $[0, T_w]$ |
| AM | $f_m$ (Hz) | 0.165 | [0.2, 5] |
| | $\varphi_m$ (rad) | 0.216 | $[0, 2\pi]$ |

the signals examined (i.e., the ground truth). 200 test signals are generated with 60 dB of white Gaussian noise for a duration of 500 ms using model parameters which are selected randomly from the following parameter ranges:

- $f_0 \in [47.5, 52.5]$ Hz
- (AM) $k_m \in [0.1, 0.7]$, $f_m \in [0.2, 5]$ Hz, $\phi_m \in [0, 2\pi]$.
- (FR) $R \in [-5, 5]$ Hz/s.
- (AS) $k_s \in \pm[0.1, 0.8]$, $t_s \in [0, 200]$ ms.
- (PS) $k_p \in \pm[\pi/18, 5\pi/18]$, $t_p \in [0, 200]$ ms.

For all tests, sliding windows of 60 ms are used with a reporting rate of 50 fps. Each signal is processed by the SCD, i-IpDFT and CSTFM algorithms, and the maximum of the following metrics are recorded:

- Time-domain error (TDE)
- Parameter error for the step components
- Frequency error (FE)
- RoCoF error (RFE)

FE and RFE represent the deviation of the estimated frequency and RoCoF from the true instantaneous frequency and RoCoF at the reporting time, conventionally located at the center of the window, as detailed in [5]. The common phasor-based metric, Total Vector Error, is not reported as it does not provide a clear indication on how good the estimation is when analyzing dynamic signals, as discussed in [8,18].

An example test is presented in Fig. 3 where a signal containing a frequency ramp of 3.92 Hz/s, and a phase and amplitude step at 0.073 s is analyzed by the proposed SCD method, the static phasor estimation method and the dynamic phasor method. When the step enters the window, the frequency values estimated by the reference techniques are highly erroneous. The maximum FE and RFE is 0.005 Hz and 0.443 Hz/s (SCD), 1.2 Hz and 110 Hz/s (static phasor) and 1.1 Hz and 102 Hz/s (dynamic phasor), respectively.

While the dynamic tests presented in the IEEE Standard [5] involve analysis of single signal dynamics, the complex signals tested here were selected to better reflect real world variations typical of power systems following grid events. Indeed, analysis of combined signal dynamics, like AS/PS/FR, is far more relevant for the LOM and UFLS applications discussed in Section 1.

The complete set of test results are presented in Table 4, showing the max and mean error for each metric. It is clear that the static and dynamic phasor analysis methods are incapable of processing signals with step changes, resulting in large frequency and RoCoF errors. The proposed algorithm, in contrast, can accurately characterized and track the step and provide a good estimate of the underlying frequency dynamic.

The SCD technique reliably identifies the location of the step to within 0.3 ms and provides an excellent estimate of the amplitude/phase step magnitude. Furthermore, when a step is present, the RFE and FE are at least one (often two) orders of magnitude smaller than the traditional static and dynamic phasor methods. Even in some of the most challenging scenarios where a phase step is combined with AM/FR, the frequency dynamic and step parameters are accurately identified. In fact, the parameter, frequency and RoCoF errors for combined dynamics are similar to the errors when a single dynamic

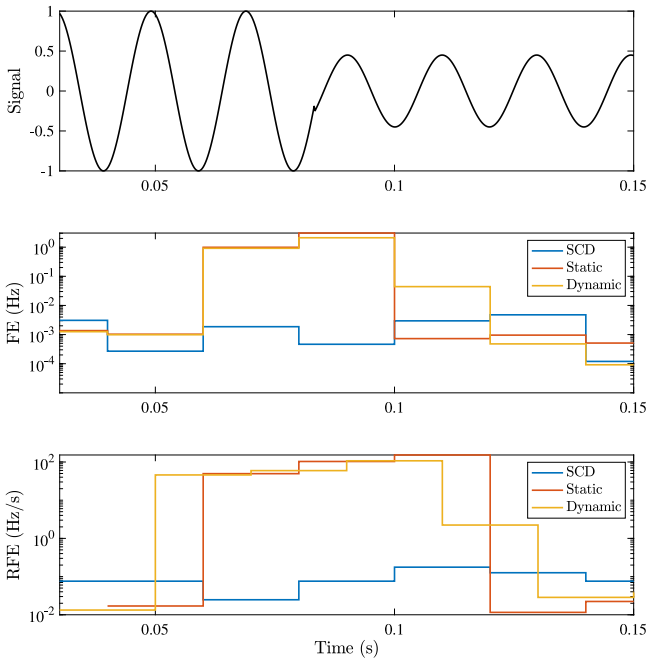


**Fig. 3.** Signal (top), FE (middle) and RFE (bottom) results for an AS/PS/FR signal ($k_p = -0.45, k_s = -0.55, R = 3.92$ Hz/s).

is analyzed. Finally, since the SCD technique includes the detected dynamic components in the reconstructed signal, the TDE is generally one order of magnitude smaller than for the other methods.

## 5. Conclusion

In this paper, we present a technique for the identification and characterization of signal dynamics in power grids with the specific goal of providing valid frequency and RoCoF estimates during amplitude and/or phase steps as well as frequency variations and harmonic interference. The proposed SCD technique exploits properties of the analytic signal and dictionaries modeling common signal dynamics to properly capture a variety of complicated signal dynamics. The method is compared with static and dynamic phasor estimation techniques and demonstrates orders of magnitude improvements in FE, RFE and time-domain reconstruction error. A critical element of the SCD method is an excellent Hilbert filter that allows for a precise approximation of the analytic form of an input signal. The development of such a filter is beyond the scope of this paper but will be the focus of upcoming research. Together with a proper Hilbert filter, the SCD method could be a powerful and flexible signal analysis method for grid monitoring and control. The SCD's ability to identify underlying frequency trends in the presence of step disturbances shows its potential for UFLS and LOM protection applications.

## CRediT authorship contribution statement

**Alexandra Karpilow:** Conceptualization, Methodology, Software, Writing – original draft. **Asja Derviškadić:** Conceptualization, Supervision, Writing – review. **Guglielmo Frigo:** Conceptualization, Supervision. **Mario Paolone:** Conceptualization, Supervision, Writing – review.

## Declaration of competing interest

The authors declare the following financial interests/personal relationships which may be considered as potential competing interests: Alexandra Karpilow reports financial support was provided by European Commission.

**Table 4**
Parameter, frequency, RoCoF and time-domain error for signal dynamic tests for the SCD technique and the static (IpDFT) and dynamic (CSTFM) phasor estimation methods.

| Dynamics | | Parameter error | | | FE (mHz) | | | RFE (Hz/s) | | | TDE | | |
|---|---|---|---|---|---|---|---|---|---|---|---|---|---|
| | | $k_x$ (%) | $k_p$ (%) | $t_s, t_p$ (ms) | SCD | Static | Dynamic | SCD | Static | Dynamic | SCD | Static | Dynamic |
| FR | Max | | | | 9 | 4 | 24 | 0.30 | 0.24 | 0.23 | 1.00E−04 | 4.70E−04 | 1.40E−04 |
| | Mean | | | | 4 | 2 | 4 | 0.12 | 0.12 | 0.08 | 9.50E−05 | 2.50E−04 | 8.80E−05 |
| AS | Max | 7.3 | | 0.2 | 14 | 920 | 853 | 0.40 | 70 | 48 | 1.40E−02 | 9.80E−02 | 6.00E−02 |
| | Mean | 1.2 | | 0.1 | 4 | 180 | 159 | 0.14 | 16 | 10.3 | 1.60E−03 | 2.10E−02 | 1.00E−02 |
| PS | Max | | 11.6 | 0.2 | 15 | 7020 | 3917 | 1.20 | 343 | 153 | 3.00E−03 | 3.80E−02 | 1.70E−02 |
| | Mean | | 2.5 | 0.1 | 7 | 2042 | 2113 | 0.38 | 161 | 78 | 1.00E−03 | 1.60E−02 | 1.00E−02 |
| AM | Max | | | | 12 | 107 | 297 | 0.30 | 5 | 8 | 9.00E−04 | 5.30E−02 | 3.50E−03 |
| | Mean | | | | 4 | 14 | 36 | 0.14 | 0.48 | 0.83 | 1.00E−04 | 1.10E−02 | 4.00E−04 |
| AS/FR | Max | 7.1 | | 0.2 | 18 | 932 | 1121 | 0.30 | 66 | 62 | 1.40E−02 | 9.90E−02 | 5.90E−02 |
| | Mean | 1.2 | | 0.1 | 5 | 182 | 163 | 0.16 | 15 | 11 | 1.60E−03 | 2.00E−02 | 1.00E−02 |
| PS/FR | Max | | 12 | 0.2 | 15 | 6991 | 3922 | 1.20 | 344 | 152 | 2.70E−03 | 3.60E−02 | 1.70E−02 |
| | Mean | | 3.6 | 0.1 | 7 | 3042 | 2022 | 0.36 | 150 | 78 | 1.30E−03 | 1.50E−02 | 9.00E−03 |
| AS/PS/FR | Max | 7.2 | 10.2 | 0.2 | 19 | 6726 | 5488 | 1.57 | 226 | 289 | 2.40E−02 | 1.00E−01 | 7.20E−02 |
| | Mean | 1.2 | 5.2 | 0.1 | 8 | 3122 | 2276 | 0.42 | 154 | 105 | 2.90E−03 | 2.70E−02 | 1.50E−02 |
| AM/PS/FR | Max | | 22 | 0.2 | 16 | 6867 | 3916 | 1.34 | 336 | 167 | 1.10E−02 | 7.90E−02 | 4.00E−02 |
| | Mean | | 3.7 | 0.1 | 7 | 3247 | 2140 | 0.35 | 160 | 84 | 2.00E−03 | 2.20E−02 | 1.10E−02 |

## References


[1] G. Rietveld, P.S. Wright, A.J. Roscoe, Reliable rate-of-change-of-frequency measurements: Use cases and test conditions, IEEE Trans. Instrum. Meas. 69 (9) (2020) 6657–6666, http://dx.doi.org/10.1109/TIM.2020.2986069.

[2] A. Derviškadić, Y. Zuo, G. Frigo, M. Paolone, Under frequency load shedding based on PMU estimates of frequency and ROCOF, 2018, http://dx.doi.org/10.1109/ISGTEurope.2018.8571481.

[3] 1,200 MW Fault Induced Solar Photovoltaic Resource Interruption Disturbance Report, Technical Report, NERC, 2017.

[4] P.S. Wright, P.N. Davis, K. Johnstone, G. Rietveld, A.J. Roscoe, Field measurement of frequency and ROCOF in the presence of phase steps, IEEE Trans. Instrum. Meas. 68 (6) (2019) 1688–1695, http://dx.doi.org/10.1109/TIM.2018.2882907.

[5] IEEE Standard for Synchrophasor Measurements for Power Systems – Amendment 1: Modification of Selected Performance Requirements, IEEE Std C37.118.1a-2014 (Amendment to IEEE Std C37.118.1-2011), 2014, pp. 1–25, http://dx.doi.org/10.1109/IEEESTD.2014.6804630.

[6] M. Paolone, T. Gaunt, X. Guillaud, et al., Fundamentals of power systems modelling in the presence of converter-interfaced generation, Electr. Power Syst. Res. 189 (2020).

[7] A.J. Roscoe, et al., The case for redefinition of fre- quency and ROCOF to account for AC power system phase steps, in: 2017 IEEE International Workshop on Applied Meas. for Power Systems (AMPS), 2017, pp. 1–6.

[8] H. Kirkham, A. Riepnieks, Dealing with non-stationary signals: Definitions, considerations and practical implications, in: 2016 IEEE Power and Energy Society General Meeting (PESGM), 2016, pp. 1–5.

[9] J.A. de la O Serna, Dynamic phasor estimates for power system oscillations, IEEE Trans. Instrum. Meas. 56 (5) (2007) 1648–1657, http://dx.doi.org/10.1109/TIM.2007.904546.

[10] M. Bertocco, G. Frigo, C. Narduzzi, C. Muscas, P.A. Pegoraro, Compressive sensing of a Taylor-Fourier multifrequency model for synchrophasor estimation, IEEE Trans. Instr. Meas. 64 (12) (2015) 3274–3283.

[11] M.B. Martins, R.T. de Barros e Vasconcellos, P.A.A. Esquef, Step change detection based on analytic signal for PMU calibrators, in: 2019 IEEE 10th International Workshop on Applied Measurements for Power Systems (AMPS), 2019, pp. 1–5, http://dx.doi.org/10.1109/AMPS.2019.8897772.

[12] M. de Ápraiz, R.I. Diego, J. Barros, Transient detection in phasor measurement units with kalman filtering, in: 2018 18th International Conference on Harmonics and Quality of Power (ICHQP), 2018, pp. 1–6, http://dx.doi.org/10.1109/ICHQP.2018.8378920.

[13] J. Ren, M. Kezunovic, An adaptive phasor estimator for power system waveforms containing transients, IEEE Trans. Power Deliv. 27 (2) (2012) 735–745, http://dx.doi.org/10.1109/TPWRD.2012.2183896.

[14] G. Frigo, D. Colangelo, A. Derviškadić, M. Pignati, C. Narduzzi, M. Paolone, Definition of accurate reference synchrophasors for static and dynamic characterization of PMUs, IEEE Trans. Instrum. Meas. 66 (9) (2017) 2233–2246, http://dx.doi.org/10.1109/TIM.2017.2698709.

[15] M.B. Martins, R.T. de Barros e Vasconcellos, P.A.A. Esquef, Models for synchrophasor with step discontinuities in magnitude and phase: Estimation and performance, IEEE Trans. Instrum. Meas. 68 (6) (2019) 2007–2014, http://dx.doi.org/10.1109/TIM.2019.2893716.

[16] A. Karpilow, A. Derviškadić, G. Frigo, M. Paolone, Characterization of non-stationary signals in electric grids: a functional dictionary approach, IEEE Trans. Power Syst. (2021).

[17] S.L. Hahn, Hilbert Transforms in Signal Processing, Artech House, 1996.

[18] A. Derviškadić, G. Frigo, M. Paolone, Beyond phasors: Modeling of power system signals using the Hilbert transform, IEEE Trans. Power Syst. (2019).

[19] European Committee for Electrotechnical Standardization, Voltage Characteristics of Electricity Supplied by Public Electricity Networks, 2010.

[20] A. Derviškadić, P. Romano, M. Paolone, Iterative-interpolated DFT for synchrophasor estimation: A single algorithm for P- and M-class compliant PMUs, IEEE Trans. Instrum. Meas. (ISSN: 0018-9456) 67 (3) (2018) 547–558, http://dx.doi.org/10.1109/TIM.2017.2779378.